

# TiNi shape memory alloy thin films for microactuator application

Yongqing Fu and Hejun Du

**Abstract**—TiNi films were prepared by co-sputtering TiNi target and a separate Ti target. Crystalline structure and phase transformation behaviors of TiNi films were investigated. Results showed that TiNi films had fine grain size of about 500 nm and fully martensitic structure at room temperature. X-ray photoelectron spectroscopy (XPS) results indicated that there is adherent and natural TiO<sub>2</sub> film, which is beneficial to its corrosion resistance and biocompatibility. Results from differential scanning calorimeter (DSC), in-situ X-ray diffraction (XRD) and curvature measurement revealed clearly martensitic transformation upon heating and cooling. The TiNi films were further deposited on micromachined silicon cantilever and membrane structures in order to form micro-gripper or microvalve with large deformation due to shape-memory effect.

**Index Terms**—TiNi thin film, Sputtering, Shape memory, Martensitic transformation

## I. INTRODUCTION

Shape memory alloys (SMAs) offer a combination of novel properties, such as shape memory effect, super-elasticity, biocompatibility and high damping capacity [1-5]. Bulk SMAs exhibit large strokes and forces but suffer from slow response. Thin film SMAs provide a larger energy density and higher frequency response, and they can be engineered into structures of micro-size dimensions, patterned with standard lithographic techniques and fabricated in batch. Thin film SMAs have potential to be a primary actuating mechanism for micro-actuators and the work output per volume of thin film SMA microactuators exceeds that of other micro-actuation mechanisms such as electrostatic, magnetic, bi-metallic, piezoelectric, and thermopneumatic, etc. However, due to lack of understanding on the properties of thin film SMAs and controlling of deposition parameters, they have not received as much attention as other microactuator technologies. Up to now, great effort has been made to produce TiNi based thin films using a sputtering technique [6-17]. Successful implementation of micro-actuators using TiNi based films requires a good understanding of the relationship among

processing, microstructure and properties of TiNi films. The shape memory characteristics of TiNi films depends significantly on metallurgical factors (such as alloy composition, annealing or aging temperatures), and sputtering conditions (such as argon gas pressure, plasma powers, substrate temperatures, etc.) [16-23]. Elaboration of various properties of TiNi films (such as the shape recovery strain, mechanical and fatigue properties, two-way shape memory effect, performance degradation, etc.) is major task, especially since the properties of SMA films are quite different from those of bulk materials.

In this investigation, TiNi films were prepared by co-sputtering of a TiNi target with a separate Ti target. Crystalline structure, phase transformation and shape memory effect of TiNi films were investigated. The TiNi films were further deposited on micromachined silicon cantilever and membrane structures in order to form a micro-gripper or microvalve with large deformation due to shape-memory effect.

## II. FILM PREPARATION

TiNi films were prepared by co-sputtering a TiNi target (with atomic percentage of Ti 50% and Ni 50%, RF power of 400W) and a separate Ti target (DC power of 35 W) on 4-inch (100) silicon substrate, which was heated to 723K during deposition. Deposition duration was 4 hours. The schematic system configuration is shown in Fig. 1. The substrate holder was rotated during deposition to achieve uniform deposition. The base pressure of the main chamber was  $1 \times 10^{-7}$  Torr. The argon pressure was 1.0 mTorr.

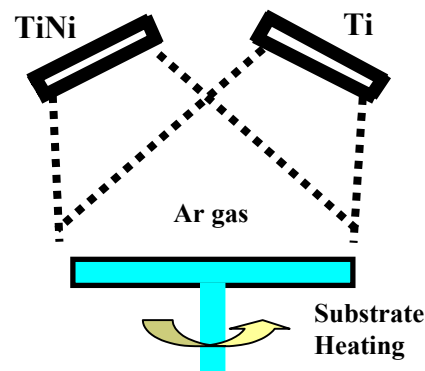


Fig. 1. Schematic show of sputtering configuration

Yongqing Fu and Hejun Du are with School of Mechanical and Production Engineering, Nanyang Technological University, Singapore, e-mail: myqfu@ntu.edu.sg.

Hejun Du is also with Advanced Materials for Micro- and Nano- Systems Programme, Singapore-MIT Alliance, Singapore (e-mail: mhdu@ntu.edu.sg).

Surface and cross-section morphology was studied by a JEOL scanning electron microscopy (SEM). Film composition was determined using energy dispersive X-ray spectroscopy (EDX). Surface structure and roughness were analyzed using a Shimadzu SFT-9800 atomic force microscopy (AFM). The internal structures of the deposited films were analyzed using a 200 kV high-resolution TEM (JEM-2000EX). XPS analysis was performed on TiNi film surface using a Kratos AXIS spectrometer with monochromatic Al K $\alpha$  (1486.71 eV) X-ray radiation. Martensitic transformation temperatures were measured using DSC (TA instrument 2920) at a heating/cooling rate of 5 K/min. The change of crystalline structure for the deposited films was analyzed using a Philips PW3719 X-ray diffractor. The curvature changes of film-deposited Si wafers were measured using a Tencor FLX-2908 laser system, and the stress changes as a function of temperature were derived with a heating and cooling rate of 0.5 K/min, from which the information about martensite transformation was obtained [14-21]. Film stress was calculated from the radius of wafer curvature using the following equations:

$$\sigma = \frac{Eh^2}{(1-\nu)6Rt} \quad (1)$$

where  $E/(1-\nu)$  is the biaxial elastic modulus of the substrate,  $h$  is the substrate thickness,  $t$  film thickness,  $R$  substrate radius of curvature.  $R$  can be calculated using the following equation:

$$R = \frac{1}{\left(\frac{1}{R_2} - \frac{1}{R_1}\right)} = \frac{R_1 R_2}{(R_1 - R_2)} \quad (2)$$

where  $R_1$  and  $R_2$  are the radius of curvature of the wafer before and after film deposition. Curvature changes of film-deposited Si wafers were measured using a Tencor FLX-2908 laser system with a heating and cooling rate of 0.5 K/min, and the stress changes as a function of temperature were derived from the above equations.

### III. FILM CHARACTERIZATION

#### 3.1. Structure characterization

Cross-section morphology of TiNi film shows some tearing features and exhibits a uniform structure without indicating column structure as shown in Fig. 2. The coating thickness is about 3.5  $\mu\text{m}$ . The composition of the film obtained from EDX is as follows: Ti: 50.3 at.%, Ni, 49.7 at.%. The variation of measured composition on the whole wafer is within  $\pm 0.5\%$ . Fig. 3 shows the surface morphology of the deposited films obtained using AFM, and the coating surface shows many tiny grains with an average size of 500 to 600 nm. The roughness value,  $R_a$ , obtained from AFM analysis is about 8 nm.

Fig. 4(a) to (d) show the high-resolution XPS spectra of Ti2p, Ni2p, O1s and C1s on surface. After deconvolution, there are eight different peaks for Ti 2p spectrum, corresponding to four chemical states from the doublet consisting of Ti 2p $_{1/2}$  and Ti 2p $_{3/2}$ . Two strong Ti $^{4+}$  peaks, i.e., 2p $_{1/2}$  (Ti $^{4+}$ ) and 2p $_{3/2}$  oxide (Ti $^{4+}$ ), two Ti $^{3+}$  peaks and two Ti $^{2+}$  peaks, as well as two metallic Ti peaks (2p $_{1/2}$  NiTi and 2p $_{3/2}$  NiTi). Ti is mostly present as TiO $_2$  state on the surface of TiNi film (about 80%). Ni mainly exists in the metallic state, while small amount of Ni $_2$ O $_3$  and NiO phases can be observed. Ni 2p spectra on film surface is shown in Fig. 4(d), in which two distinct metallic Ni peaks of Ni 2p $_{3/2}$  (852.6 eV) and Ni 2p $_{1/2}$  (869.9 eV) are observed. Other weak peaks are correspondent to Ni $^{3+}$  (i.e., Ni $_2$ O $_3$ , 853.8 eV) peak and Ni $^{2+}$  (i.e., Ni(OH) $_2$ , 855.4 eV) peak. O 1s binding energy region around 530 eV is shown in Fig.4 (c). There are two peaks, one is identified as strong O $^{2-}$  peak (at 530.5 eV) and another weak but broad peak is attributed to a combination of OH $^-$  (at 531.5 eV) and chemisorbed water H $_2$ O (at 533 eV). Apart from O, there is also significant carbon chemisorption as shown in Fig. 4(d). The carbon adsorption is characterized by a strong C-C bond (285 eV), and a weak C-H peak (287 eV, corresponding to the presence of hydrocarbon) and C-O peak (289.4 eV), etc. Most carbon were involved in C-C bonds (284.8 eV), which is from contamination of atmospheric hydrocarbon-rich. Surface composition is as follows: oxygen 36.92 at%, Ti 31.03 at%, Ni 18.54 at%, and carbon 13.51 at%.

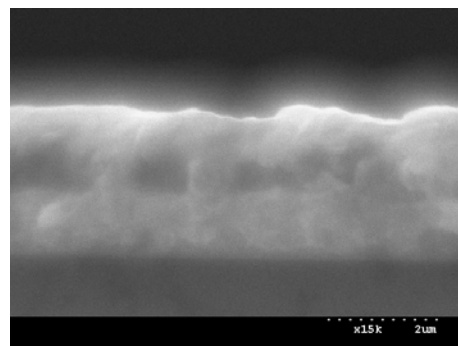


Fig. 2. SEM cross-section of TiNi film

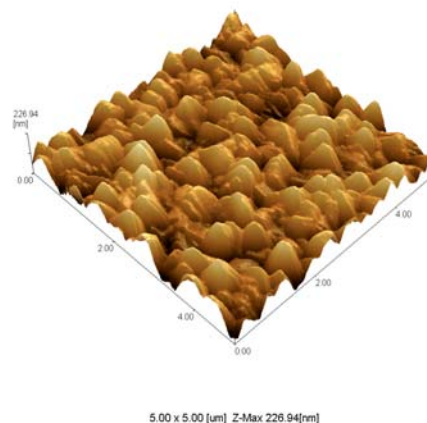


Fig. 3. AFM surface morphology of TiNi film

High nickel content in TiNi based alloys often causes the doubt of its successful medical use. The presence of an adherent and stable TiO<sub>2</sub> oxide layer on TiNi film can prevent Ni element to release from surface, which is beneficial to its corrosion resistance and biocompatibility. However, it was reported that this passivation layer on bulk NiTi alloy was relatively fragile [24]. The mechanical properties of TiO<sub>2</sub> and TiNi are quite different, and this brittle and thin oxide layer may be destroyed during significant deformation or during complex interaction involving wear [24,25]. Therefore, the stability and ductility of this native formed oxide layer has to be considered in the implant design. The optimized preparation and modification processes for this passivation layer, and prevention of surface layer degradation are crucial from the point of view for TiNi thin film medical applications.

TEM micrograph of the deposited films reveals that the grain size of martensite is about 500 nm. The fine grain size is characteristic of sputtered thin films if compared with the grain size of several tens of microns for bulk materials. Fig. 5 shows a high magnification TEM image of the TiNi thin film, in which finely twinned B19' monoclinic martensite dominates at room temperature. There are two main types of martensite variants which consist of <011> type II and <11-1> Types I twins as shown in Fig. 5. <011> type II twins are most frequently observed in our study. During martensitic transformation, <011> type II twins appear first since there is no elastic strain at the beginning of the transformation. The interaction may arise between or inside each variant due to the growth of these variants, then the elastic strain is induced, resulting in the <11-1> type I twins, with spear-like morphology at the junction area shown in Fig. 5.

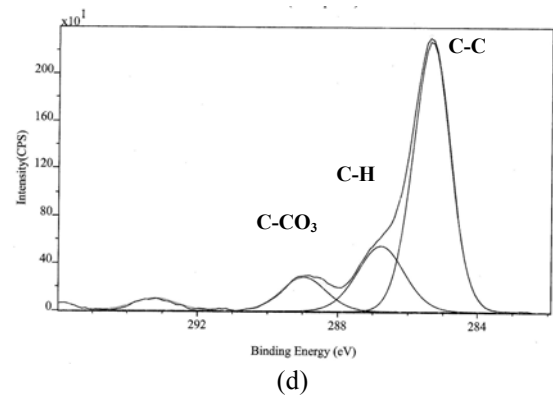
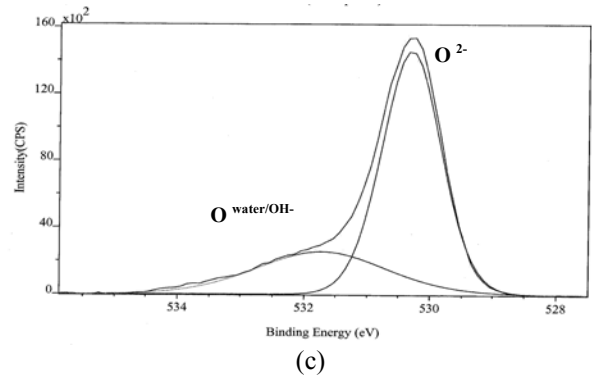
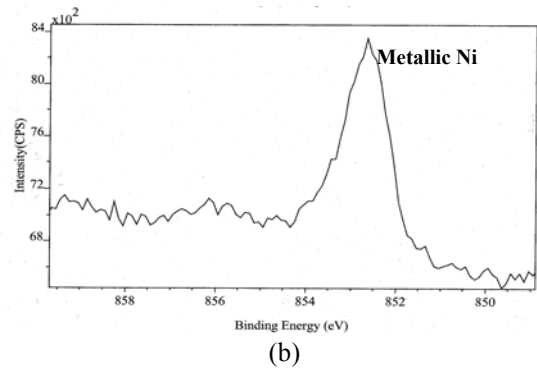
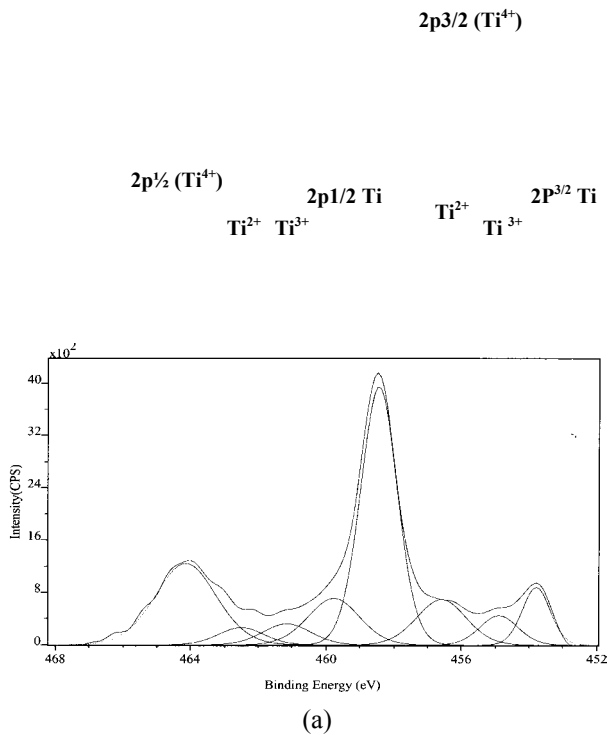


Fig. 4. XPS analysis results for the TiNi film

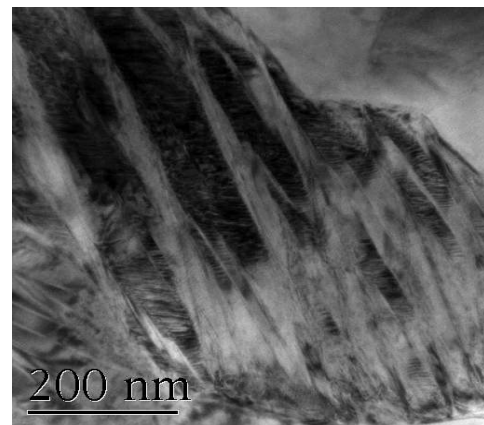


Fig. 6. TEM morphology of the martensite plates

### 3.2. Martensite transformation

Fig. 6 shows the DSC result of TiNi films. During heating, a one-stage transformation is observed, corresponding to B19' to B2 transformation. During cooling, a two-stage transformation is observed, corresponding to transformations among B2, R-phase and B19' phase.

XRD analysis results are shown in Fig. 7. At room temperature, film structure is mainly martensite (B19', monoclinic). With the increase of temperature, martensite phase gradually changes to austenite as shown in Fig. 7(a), without much evidence of existence of R-phase (rhombohedral phase). During the cooling process, the changes of diffraction patterns reveal clearly B2 to R phase transformation as shown in Fig. 7(b), respectively. The heights and widths of (011)<sub>B2</sub> peak decrease and broaden, and gradually split into two resolvable (112)<sub>R</sub> and (300)<sub>R</sub> peaks with the decrease of temperature. With the further decrease in temperature, the remained austenite and R-phase gradually change to martensite.

Fig. 8 shows stress evolution as a function of temperature for TiNi film. The stress vs. temperature plot shows a closed hysteresis loop. During heating, the stress increases significantly at a rate of about 17.5 MPa/K due to phase transformation from martensite to austenite, which forms the basis for cyclic actuation of the SMA/Si composites applicable to MEMS. The effect of applied stress on shape memory behavior can be derived from a thermodynamic approach using the famous Clausius-Clapeyron equation:

$$\frac{d\sigma}{dT} = -\frac{\Delta S}{\epsilon} = -\rho \frac{\Delta H}{\Delta \epsilon T_0}$$

where  $d\sigma/dT$  is the temperature coefficient of the critical stress for the transformation,  $\Delta \epsilon$  is the amount of strain due to the stress-induced martensite transformation,  $\rho$  is the density of the alloy,  $\Delta S$  and  $\Delta H$  are the transformation entropy and enthalpy (or heat) of transformation ( $\Delta H$  is 14.7 J/g from DSC tests).  $T_0$  means the temperature at which Gibbs free energy of austenite equals to that of martensite, usually represented as  $(M_s + A_f)/2$  [27] (roughly 338K in our study). If taking the theoretical transformation shear of 0.047 and material density of 6.54 g/cm<sup>3</sup> [28], the estimated biaxial stress rate is about 6.1 MPa/K. This value is much smaller than the experimental data, which shows that thermodynamic approach using Clausius-Clapeyron equation is not applicable for stress evolution during phase transformation in this study. With the further increase of temperature above austenite transition finish temperature ( $A_f$ ), the transformation completes and the generation of thermal stress occurs with the stress values decreasing linearly.

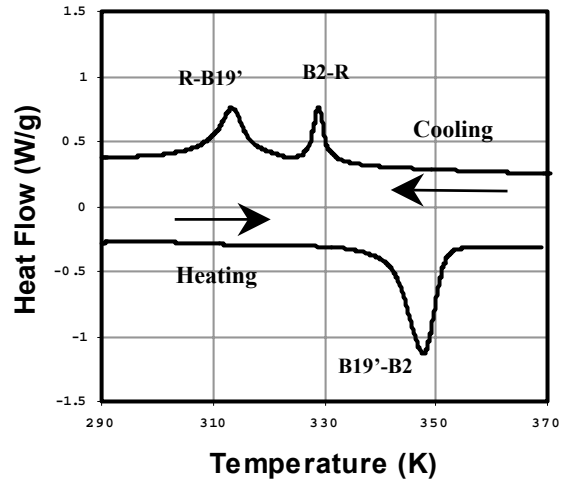
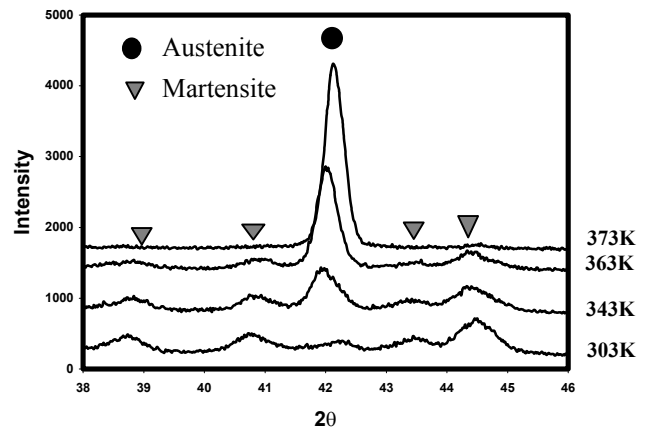


Fig. 6. DSC results of TiNi films

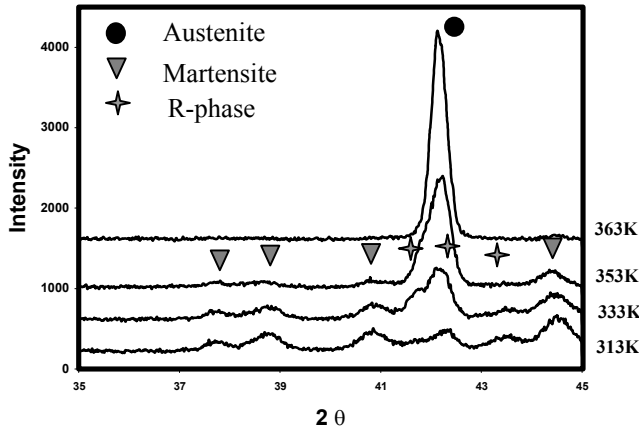
During the cooling process from 373 K, tensile thermal stress develops in TiNi films at a rate of  $-1.45$  MPa/K due to the difference in coefficient of thermal expansion (CTE) between TiNi film ( $\alpha = 15.4 \times 10^{-6}/K$ ) and Si substrate ( $\alpha_{Si} = 3 \times 10^{-6}/K$ ) [21]. If the Young's modulus of TiNi film is chosen as 82 GPa (for austenite phase), and Poisson ratio of TiNi film of 0.33, then the calculated data of  $d\sigma/dT$  is about  $-1.44$  MPa/K using the following equation, which agrees well with the measured value.

$$D\sigma/dT = [E_{TiNi}/(1-\nu_{TiNi})](\alpha_{Si}-\alpha_{TiNi})$$

When the temperature is just above martensite transition start temperature ( $M_s$ ), the residual stress reaches its maximum value, 320 Mpa in this case. Cooling below  $M_s$ , the martensitic transformation occurs and the tensile stress drops significantly due to the formation and alignment of twins, shear-variant boundary motion and stress-induction of low-symmetry phases. There is a small hump during cooling processes, indicating that there may exist a two-step transformation. The recovery stress,  $\sigma_{rec}$ , given by the difference between the maximum and minimum stress, is about 350 MPa.



7(a)



7(b)

Fig. 7. XRD analysis results with the change of temperature during (a) heating and (b) cooling processes

The stability of stresses during heating and cooling around phase transformation temperatures are very important since they will affect shape memory effect and the performance of force-producing MEMS systems. The cyclic stress relaxation and recovery and the associated hysteresis have important consequences for exploitation of shape-memory thin films in MEMS applications. TiNi films on Si wafer was used in thermal cycling tests with a heating/cooling rate of 0.5 K/min and a temperature range from 313 and 353 K. Results showed that during cycling, the recoverable stress gradually decreases as shown in Fig. 9. This reduction of the recoverable stress is probably due to the dislocations, grain boundaries sliding, void formation, or partial decohesion at the film/substrate interfaces, etc. This reduction in recoverable stress is more severe in the early cycles, but gradually slows down after 20 cycles. Fig. 9 shows the recovery stress with the cycling cycles, and the recoverable stress drops from 355 MPa to 335 MPa after 100 cycles, to 330 MPa after 200 cycles. The reduction of residual stress is not apparent after 1000 cycles.

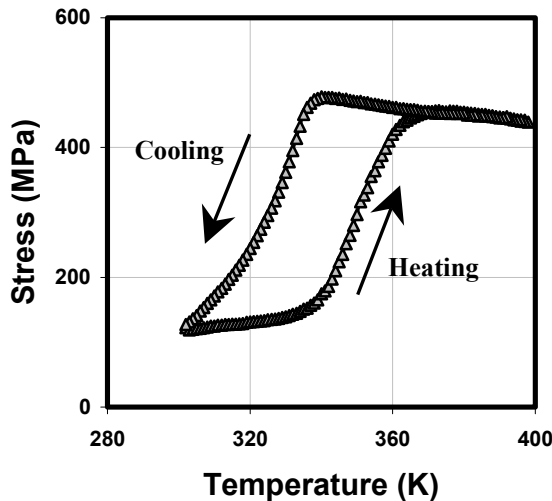


Fig. 8. Stress evolution curves during martensite transformation as a function of temperature

#### IV. MICROACTUATOR APPLICATION

To evaluate the shape-memory effect, a silicon cantilever structure with a thickness of 15 μm (see Fig. 10) was fabricated using a bulk micromachining process. By depositing TiNi films on this Si cantilever, we can obtain micro-beams exhibiting the shape-memory effect. A hot plate was used to heat the TiNi/Si cantilever. This TiNi/Si cantilever structure was heated to different temperatures and the deflection of the cantilever tip can be seen clearly. The tip displacement is quite large (up to 60 μm). This type of cantilever structure can be further fabricated as a micro-gripper, which can be actuated at relatively low temperatures with internal integrated heaters formed by polysilicon patterns [22]. These grippers can be used as the end-manipulator for micro-assembly for industry, minimally invasive surgery for medical application, and handling of small particles in hazardous environment for military application.

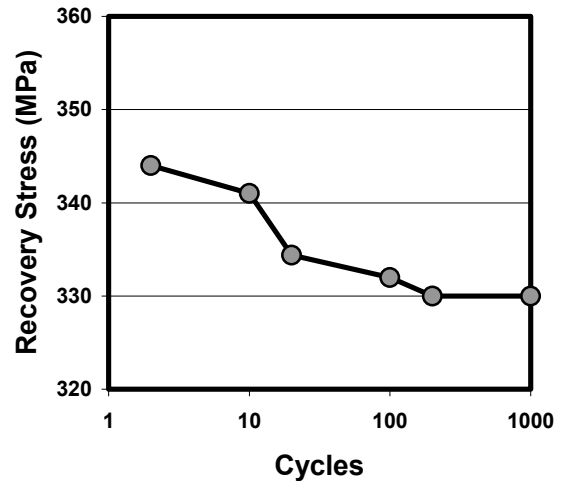


Fig.9. Recovery stress changes with heating and cooling cycles

A membrane structure (1.5mm × 1.5mm) was fabricated using deep reactive ion etching (DRIE), and the results are shown in Fig. 11. TiNi film was then deposited on top of the membrane structure. When heated, the SMA/Si bimorph diaphragm will show shape memory effect. It is flat at room temperature, and turn to concave when TiNi film is heated to high temperature.

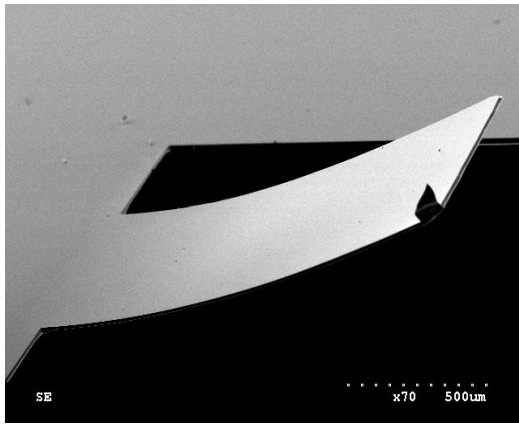


Fig. 10. TiNi deposited micro-cantilever when heated showing shape memory effect

When cooled from austenite, martensite phase transformation occurs, stress and curvature drops significantly. Self-accommodation variants of martensite forms, causing a macroscopic shape change, and the thermal stress in the bimorph system is also relaxed. The membrane becomes flat. When temperature increased, martensite to austenite transformation occurs. Thus tensile stress develops and thermal stress also occurs in the films, causing the returning of shape memory. The advantages of using SMA/Si membrane is that no special bias structure is needed because the silicon substrate can provide bias force.

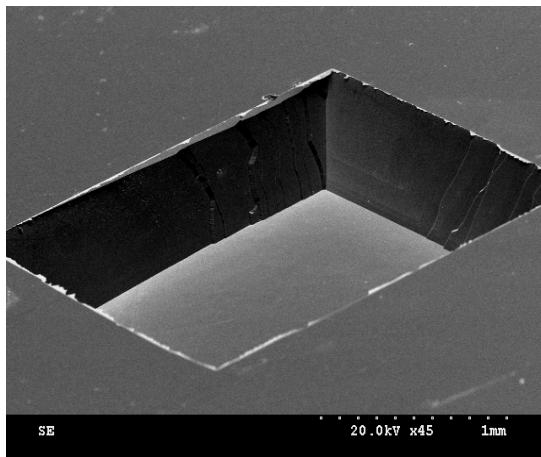


Fig. 11. Si membrane fabricated using bulk micromachining

TiNi film was then further patterned with photolithography, then etched using HF:HNO<sub>3</sub>:H<sub>2</sub>O solution to form electrode as shown in Fig. 12. The micropump is composed of a TiNi/Si bimorph, one chamber and two inlet and outlet check valves, as schematically shown in Fig. 13. When the patterned TiNi electrodes are heated by electric currents, an effective shape memory effect is generated. This would cause the pressure of the pump chamber to increase and decrease so that the working fluid will be sucked in and pushed out through the check valves. This work is still in progress.

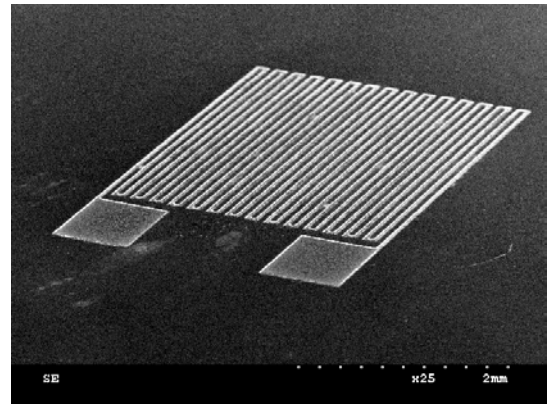


Fig. 12. TiNi electrode (on Si membrane) fabricated using wet etching in HF:HNO<sub>3</sub>:H<sub>2</sub>O solution

## V. CONCLUSION

TiNi films had fine grain size of about 500 nm and fully martensitic structure at room temperature. X-ray photoelectron spectroscopy (XPS) results indicated that there is adherent and natural TiO<sub>2</sub> film, which is beneficial to its corrosion resistance and biocompatibility. Results from differential scanning calorimeter (DSC), in-situ X-ray diffraction (XRD) and curvature measurement revealed clearly martensitic transformation of the deposited TiNi films upon heating and cooling. The TiNi films were further deposited on micromachined silicon cantilever and membrane structures in order to form micro-gripper and microvalve with large deformation due to shape-memory effect.

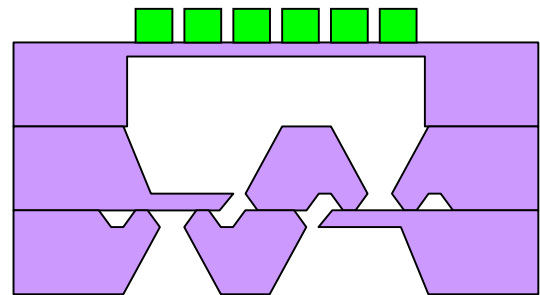


Fig.13. The proposed TiNi based micro-pump structure

## REFERENCES

- [1] R. H. Wolf and A. H. Heuer, *Journal of Microelectromechanical Systems*, 4 (1995) 206.
- [2] C. M. Wayman, *Progress in materials Science*, 36 (1992) 203.
- [3] H. Kahn, M. A. Huff and A. H. Heuer, *J. Micromech. Microeng.*, 8 (1998) 213.
- [4] S. Miyazaki, A. Ishida, *Mater. Sci. Engng. A* 273-275 (1999) 106.
- [5] Z. G. Wei, R. Sandstorm and S. Miyazaki, *J. Mater. Sci.* 33 (1998) 3743.
- [6] P. Krulevitch, A. P. Lee, P. B. Ramsey, J. C. Trevino, J. Hamilton, M. A. M. A. Northrup, *J. MEMS*, 5 (1996) 270.
- [7] T. Lehnert, S. Crevoiserat, R. Gotthardt, *J. Mater.Sci.*, 37 (2002) 1523-1533.



- [8] T. Lehnert, H. Grimmer, P. Boni, M. Horisberger and R. Gotthardt, *Acta Mater.* 48 (2000) 4065.
- [9] P. Krulevitch, P. B. Ramsey, D. M. Makowiechi, A. P. Lee, M. A. Northrup and G. C. Johnson, *Thin Solid Films*, 274 (1996) 101.
- [10] E. Quandt, C. Halene, H. Holleck, K. Feit, M. Kohl, P. Schloßmacher, A. Skokan and K.D. Skrobanek, *Sensors and Actuators, A* 53 (1996) 434.
- [11] T. Matsunaga, S. Kajiwara, K. Ogawa, T. Kikuchi, S. Miyazaki, *Mater. Sci. Engng. A* 273-275 (1999) 745.
- [12] J. L. Seguin, M. Bendahan, A. Isalgue, V. Esteve-Cano, H. Carchano, V. Torra, *Sensors and Actuators A*, 74 (1999) 65.
- [13] A. Ohta, S. Bhansali, I. Kishimoto, A. Umeda, *Sensors and Actuators*, 86 (2000) 165.
- [14] D. S. Grummon, *Mater. Sci. Forum*, 327-328 (2000) 295.
- [15] W. L. Benard, H. Kahn, A. H. Heuer and M. A. Huff, *J. of MEMS*, 7 (1998) 245.
- [16] C. L. Shih, B. K. Lai, H. Kahn, S. M. Philips, A. H. Heuer, *J. MEMS*, 10(2001) 69.
- [17] Y. Q. Fu, W. M. Huang, H. J. Du, X. Huang, J. P. Tan, X. Y. Gao, *Surf. Coat. Technol.* 145 (2001) 107.
- [18] D. S. Grummon, J. P. Zhang, T. J. Pence, *Mater. Sci. Engng.*, A273-275 (1999) 722.
- [19] Y. Q. Fu, H. J. Du, *Surface and Coatings Technology*, 153 (2002) 100.
- [20] Y. Q. Fu, H. J. Du, *Materials Science and Engineering A*, 339 (2002) 10.
- [21] Y. Q. Fu, H. J. Du, *Materials Science and Engineering A*, 342 (2002) 237-245.
- [22] A. L. Roytburd, T.S. Kim, Q. Su, J. Slutsker, M. Wuttig, *Acta Mater.*, 14 (1998) 5095.
- [23] A. Ishida, M. Sato, A. Takei, S. Miyazaki, *Mater. Trans. JIM*, 36 (1995) 1349.
- [24] P. Filip, J. Lausmaa, J. Musialek, K. Mazanec., *Biomaterials*, 32 (2001) 2131.
- [25] S. M. Green, D. M. Grant, J. V. Wood, *Mater. Sci. Engng.*, A 224 (1997) 21
- [26] P. Surbled, C. Clerc, B. L. Pioufle, M. Ataka, H. Fujita, *Thin Solid Films*, 401 (2001) 52.
- [27] A.L. Mckelvey and R.O. Ritchie, *Philosophical Magazine A*, 80 (2000) 1759.
- [28] J. Perkins, R.O. Sponholz, *Metall. Trans. A*, 15 A (1984) 313

**Dr Yongqing Fu** obtained his Ph.D. degree from Nanyang Technological University, Singapore, in 1999. Now he is a research fellow in School of MPE, Nanyang Technological University. His research interests are in surface coatings and thin films and MEMS.

**A/P Hejun Du** obtained his both BEng and MEng from Nanjing University of Aeronautics and Astronautics, China in 1983 and 1986, respectively. He received his PhD from Imperial College of Science, Technology and Medicine, UK in 1991, before joined Nanyang Technological University, Singapore. Du's research interests mainly include two areas: 1) numerical and computational methods for engineering applications; 2) MEMS sensors and actuators. He joined SMA as a fellow in 2002.